Proceedings of ASME Turbo Expo 2011
GT2011
June 6-10, 2011, Vancouver, British Columbia, Canada

GT2011-46728

AERODYNAMIC IMPROVEMENTS OF WIND-TURBINE AIRFOIL GEOMETRIES WITH THE PRESCRIBED SURFACE CURVATURE DISTRIBUTION BLADE DESIGN (CIRCLE) METHOD

T. Korakianitis,* M. A. Rezaienia, I. A. Hamakhan, E. Avital, J. J. R. Williams
School of Engineering and Materials Science
Queen Mary, University of London
London, E1 4NS, UK

ABSTRACT

The prescribed surface curvature distribution blade design (CIRCLE) method can be used for the design of two-dimensional (2D) and three-dimensional (3D) turbomachinery blade rows with continuous curvature and slope of curvature from leading edge (LE) stagnation point to trailing edge (TE) stagnation point and back to the LE stagnation point. This feature results in smooth surface pressure distribution airfoils with inherently good aerodynamic performance. In this paper the CIRCLE blade design method is modified for the design of 2D isolated airfoils. As an illustration of the capabilities of the method, it is applied to the redesign of two representative airfoils used in wind turbine blades: the Eppler 387 airfoil; and the NREL S814 airfoil. Computational fluid dynamic analysis is used to investigate the design point and off-design performance of the original and modified airfoils, and compare with experiments on the original ones. The computed aerodynamic advantages of the modified airfoils are discussed. The surface pressure distributions, drag coefficients, and lift-to-drag coefficients of the original and redesigned airfoils are examined. It is concluded that the method can be used for the design of wind turbine blade geometries of superior aerodynamic performance.

NOMENCLATURE

b axial chord (nondimensionally b=1)
c axial chord, leading to trailing edge
$c_0, c_1 \ldots$ thickness coefficients (eqns. 3,5)
$C1, C2 \ldots$ Bezier control points (fig. 4d)
$\mathbf{C} = 1/r$ curvature (eqn. 1 and fig. 4d)
C_D drag coefficient
C_L tangential-loading (lift) coefficient
C_p pressure coefficient
i incidence
$k_1, k_2 \ldots$ exponential polynomials (eqns. 3,5)
M Mach number
o throat circle (fig. 4a)
p pressure
P points or nodes on the blade surfaces
r local radius of curvature (eqn. 1)
Rey Reynolds number
S tangential pitch of the 2D blades (fig. 4)
(x, y) Cartesian coordinates
(X, Y) nondimensionalized coordinates (with b)
$y1$, $y2$ $y3$ airfoil segments: leading edge; main part; and trailing edge (fig. 4)

Greek
α flow angle
β blade-surface angle
λ stagger angle of the blades
ϕ angle of throat diameter (fig. 4)

Subscripts
a atmospheric
crd chord line
in inlet region
ot outlet region
p pressure side

*Corresponding author. Email forward for life: *korakianitis@alum.mit.edu*

$p2$ pressure side point, TE circle to $y1$ segment (fig. 4)
pm pressure side point, $y1$ to $y2$ segments (fig. 4)
pk pressure side point, $y2$ to $y3$ segments (fig. 4)
$p1$ pressure side point, $y3$ segment to LE circle (fig. 4)
s suction side
$s2$ suction side point, TE circle to $y1$ segment (fig. 4)
sm suction side point, $y1$ to $y2$ segments (fig. 4)
sk suction side point, $y2$ to $y3$ segments (fig. 4)
$s1$ suction side point, $y3$ segment to LE circle (fig. 4)
t thickness distribution (eq. 5)

INTRODUCTION

Flow conditions

Despite their serene appearance and graceful motion, horizontal and vertical axis wind turbines are extremely dynamic structures under the influence of unsteady forces because they are operating under complex and unsteady distributions of aerodynamic loading. Wind blowing over a flat area of the earth creates an atmospheric boundary layer of thickness of the order of 200 m or sometimes higher, while atmospheric turbulence varies with local wind speed. The power that can be produced from a wind turbine is proportional to the projected area of the turbine, or the square of turbine diameter, and proportional to the cube of incoming flow velocity. In order to maximize the power per wind turbine, the combination of these factors leads to increasingly larger turbine diameters. Current wind turbines range from under a meter to well over 125 meters in diameter. The larger turbines operate at much higher incoming-freestream velocities: at the bottom of its travel the blade tip is well within the atmospheric boundary layer (relatively lower incoming velocity), while at the top of its travel it is closer to the freestream, and the incoming velocity to the blade tip is much higher. Therefore incoming velocity and turbulence are different at the top and bottom of blade-tip travel. A third source of unsteadiness is the passing of the rotor blades upstream of the tower (potential-flow interaction). Freestream velocities and directions are different depending on whether patterns and terrain. Though wind-turbine blades are designed for a “design point”, they operate at off-design point practically all the time. Therefore wind turbine blades must be designed to operate efficiently at widely different incidences and turbulence levels.

Wind turbine blades are designed by stacking 2D isolated airfoil sections, with substantial changes in thickness and type of 2D section from hub to tip. As the blades have to operate in a wide range of incoming freestream velocity and turbulence levels, and operate for most of the time at “off design” conditions, compromises must be made. The choice of 2D sections are not necessarily chosen for airfoil-incidence levels corresponding to an individual airfoil’s maximum value of lift-to-drag ratio (C_L/C_D) at “design point”. Airfoils are selected based on their performance at the required Reynolds numbers. The operating Reynolds number varies for different applications (a scaling effect). For instance at sea level insects fly at $Rey = 10^2$ to 10^4, birds at 10^4 to 10^5, wind turbines operate at 10^4 to 10^6, and wings for large civil aircraft operate at 10^7 to 10^8. Depending on Rey the flow over an airfoil may be: laminar from leading edge (LE) to trailing edge (TE); or may start laminar near the LE and transition to turbulence somewhere along the airfoil surface; or in high Rey it may transition to turbulence very near the LE, or be turbulent throughout the length of the airfoil. In all cases dominant factors are: the lift to drag ratio C_L/C_D; the loading on the airfoil; the loading distribution along the chord (determined by the C_p distribution along X or equivalent parameter); and the behavior of the boundary layer as it develops over the airfoil surfaces, which depends heavily on Rey. At low Rey the viscous effects are relatively large.

The suction surface introduces higher velocity and lower pressure. The eventual return to freestream pressure near the trailing edge implies an adverse pressure gradient from the maximum velocity/minimum pressure point along the suction surface to the trailing edge. For $Rey > 10^6$ and at design point this adverse pressure gradient normally occurs after transition, in a turbulent boundary layer that can negotiate reasonable adverse pressure gradients without separation. However, for lower Rey airfoils, the boundary layer at the beginning of the adverse pressure gradient may still be laminar, and therefore unable to withstand significant adverse pressure gradients. When a laminar boundary layer separates, the separated layer frequently undergoes transition to turbulence because the low momentum fluid mixes with higher momentum fluid in the free shear layer, making it possible for the flow to re-attach as a turbulent boundary layer, resulting in what is referred to as a “laminar separation bubble with turbulent reattachment”. The distance from separation to reattachment is such that in airfoils of $Rey < 50 \times 10^3$ the flow usually does not re-attach until after the trailing edge, with consequent implications for reduction in C_L/C_D (fig. 1). Blade surface roughness adds to friction and therefore drag, but it has different effects on laminar and turbulent boundary layers; and it can induce turbulence in boundary layers near separation, thus stabilizing boundary layer behavior (fig. 1). The wide variation in incidence has additional effects on turbulence, and in order to use them in wind turbines additional aerodynamic tests are required even for airfoils of “known” performance (e.g. [1]).

Airfoil shapes

A large variety of airfoil section geometries has been developed for different applications, some in the shape of teardrops, others in paisley shapes, and others in even more esoteric shapes [2, 3]. Initially wind-turbine airfoils were based on other aeronautics applications, e.g. NACA series with thickness distributions, but later (in addition to traditional airfoils) other airfoils dedicated to wind turbines were developed by SERI, NREL, Risø and others. Some of these airfoils are specialized for larger wind turbines (e.g. [4, 5]), others are specialty airfoils for small wind turbines (e.g. [6]), and their modifications (e.g. [7]). Inverse design methods are increasingly used for the optimization of wind turbine airfoils (e.g [8–11]). Inverse design methods have a difficulty at the stagnation points near the LE and TE of airfoils where nominally velocity is zero (singularity). Unique among these is the method described in [10], in which one Bezier-type curve with several control points is used to design the airfoil from TE to suction around the LE and back to the pointed TE. This method still uses pointed trailing edges. By its nature it provides curvature continuity throughout the airfoil surfaces and the LE. It does not give the designer exact control of the minimum X location of the LE, but this is not a limitation because the airfoil coordinates are easily re-scaled for the desired chord length. Other inverse methods result in blades with zero thickness at the trailing edge, which are impossible to manufacture; or with other adaptations made at the trailing edge introducing uncertainties. It may be difficult to obtain an acceptable geometry with an inverse method [12–15].

Leading edge (LE) separation bubbles are a frequent occurrence at design and off-design conditions throughout the *Rey* range, leading to adverse boundary-layer development implications further downstream (and on the suction as well as pressure surfaces) in all types of turbomachines [16–20]. This is related to the "double-stall" phenomenon in airfoils [21, 22]. Previous work has been done on the redesign of airfoils in order to improve aerodynamic performance with specific reference to double stall [23]. This LE separation bubble issue is exacerbated by the rate of change in surface curvature where the LE circle joins the thickness distribution describing the airfoil surface. Separation bubbles create losses, and in order to reduce these losses there is a desire to design airfoils that resist the creation of separation bubbles. There is therefore a need for a method to remove the surface curvature "disturbances" or "kinks" in that region in order to reduce the aerodynamic implications of LE separation bubbles at design and off-design incidence, throughout the *Rey* range.

The local surface curvature distribution of the airfoil and surface roughness affect the boundary layer behavior. While surface roughness and fouling promote turbulence and may energize the boundary layer, in some cases reducing overall losses [25, 26], kinks and discontinuities in surface curvature distribution in the as-designed surface have an adverse effect on boundary layer behavior, and therefore act to increase airfoil losses. As will be seen later in this paper the airfoil surface may appear smooth where the surface curvature is not smooth, and surface curvature distribution is dominant in determining the state of boundary layer development. For instance an unseparated boundary layer over the suction surface over points A, C and D is illustrated in fig. 2a. An airfoil of higher loading with separated flow is illustrated in fig. 2b, where separation is about to begin at point B. The blade surfaces (x, y) and surface curvature distributions $(x, \mathbf{C})$ of two slightly different airfoils at points such as B in fig. 2b, where the boundary layer is near separation, are illustrated in fig. 3. Such slope of curvature discontinuities can result from airfoils whose geometries appear practically identical ([27–31]), but they affect boundary layer development if they occur near points such as B, and also throughout the boundary layer development, from LE to TE.

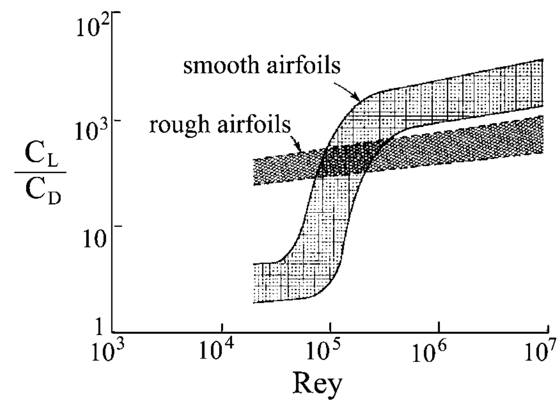

FIGURE 1. Effect of Reynolds number and surface roughness on airfoil C_L/C_D (adapted from [24])

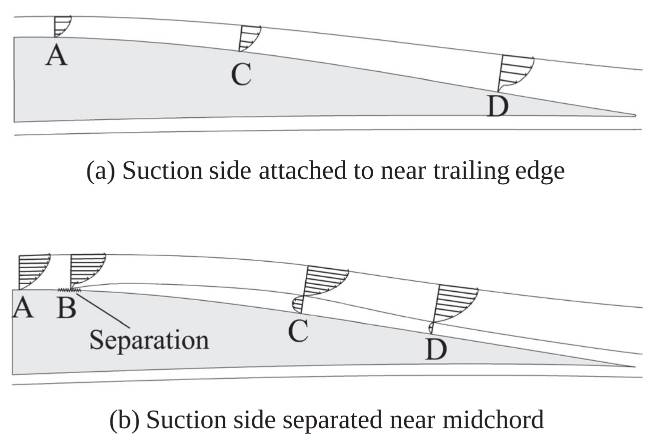

FIGURE 2. Good and bad boundary layers on airfoil

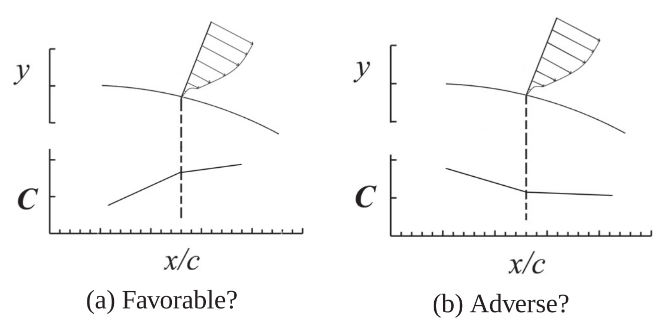

FIGURE 3. Curvature $\mathbf{C}$ (defined by eq. 1) and y, or y' or y'' continuity are not similar quantities

Therefore, the purpose of this paper is to introduce a new direct airfoil design (or re-design) method in which the airfoil *by specification* has continuous curvature $\mathbf{C}$ and continuous slope of curvature $\mathbf{C}'$ throughout the airfoil shape, and is therefore of inherently good aerodynamic performance. This $\mathbf{C}$ and $\mathbf{C}'$ continuity is imposed along both suction and pressure surfaces, through the LE and TE shapes, and through the stagnation points (where the LE stagnation point may be different from the geometric LE). The designer can choose to produce an airfoil geometry appearing identical to the geometry of the original airfoil (thus approximately maintaining maximum camber and thickness locations), or a totally different airfoil. This method is based on modifications to the earlier 2D turbine-blade design method [27–31] and its 3D extensions [32], and can be coupled with various hybrid multi-objective genetic, heuristic and evolutionary-algorithm optimization techniques in order to optimize various aspects of airfoil performance. The advantages of the proposed airfoil design method are illustrated with two examples of redesigns of two representative wind-turbine airfoils.

IMPORTANCE OF AIRFOIL CURVATURE DISTRIBUTION

The boundary layer does not shield the core of the flow from as-designed surface curvature discontinuities. The working fluid does not move over the airfoil along Cartesian coordinates, but curves around it. When the core flow as well as the boundary layer equations are written in curvilinear coordinates, the equations show local pressure on the airfoil surface has a strong dependence on local radius of curvature. Smooth streamwise surface-pressure distributions (avoiding local accelerations and decelerations) require smooth surface-curvature distributions (continuous slopes of pressure and curvature along the airfoil surface). The theoretical and experimental evidence of this statement is presented in detail in previous publications [29–31]. One must distinguish here between surface roughness and fouling, with which turbines must operate, and the slope-of-curvature discontinuities in the as-designed shape at the junctions of the splines. The latter are invisible to the eye (the blade looks very smooth), but they may produce unusually-loaded blades and thicker wakes. Continuous slope of curvature requires continuous third derivatives at the splines or surface patches used to design the blades. The importance of third-derivative continuity at the spline knots is illustrated by the following equations for $\mathbf{C}$ and $\mathbf{C}'$, where $y = f(x)$, $y' = df(x)/dx$, $y'' = d^2f(x)/dx^2$ and $y''' = d^3f(x)/dx^3$.

$$\mathbf{C} = \frac{1}{r} = \frac{y''}{[1+y'^2]^{(3/2)}} \tag{1}$$

$$\mathbf{C}' = \frac{d\mathbf{C}}{dx} = \frac{y'''\left[1+y'^2\right] - 3y'y''^2}{[1+y'^2]^{(5/2)}} \tag{2}$$

$\mathbf{C}$ and $\mathbf{C}'$ discontinuity effects are visible as small local "kinks" in surface pressure or isentropic Mach number distributions in some of the computational and experimental data published, for example, in [33–36], and with local separation bubbles in [37–40]. Even more blades and airfoils present a slope of curvature discontinuity where the LE circle or other shape joins the main part of the blade, causing in many cases leading edge separation bubbles and discontinuities, which also affect aerodynamic performance. These have been recently systematically studied in compressor leading edges [41, 42]. Such a local leading-edge laminar-separation bubble due to blending of a leading-edge circle with the blade surfaces occurs in the turbine geometry published in [38], seen in the test data published in figure 11 of [40]. This leading-edge separation region was removed by modifying the geometry of the blade in the vicinity of the slope-of-curvature discontinuity with an inverse design technique as explained in figures 11, 12 and 13 of [43]. This is a particularly challenging leading edge separation bubble because of the combination of inflow angle and large changes of curvature in the LE region. Previous attempts with parametric direct blade-design methods to remove this leading edge separation bubble have indicated difficulties [44]; however, with the CIRCLE method we have produced a slightly modified blade geometry that removes this separation bubble [45].

2D AND 3D BLADE AND AIRFOIL DESIGN

The CIRCLE method was originally developed for the design of 2D and 3D gas turbine blades [27–32], and later modified for the design of 2D and 3D compressor blades. Sample 2D and 3D compressor and turbine examples are presented in [46]. This paper presents the modifications of the method for 2D isolated airfoils, and examines the resultant airfoil performance as a function of incidence. The CIRCLE method for 2D turbine blades is summarized below, in order to later outline the modifications made for isolated airfoils, and to facilitate discussion of the results.

Fig. 4 illustrates the CIRCLE method for 2D gas turbine blades. The suction and pressure sides are each divided in three segments, $y1, y2$ and $y3$, which are joined to the LE and TE shapes. Compressor and turbine blades are set at stagger angle λ (fig. 4a), while for isolated airfoils this is set to λ=0 (fig. 4e). Compressor and turbine geometries are defined on the suction side by the minimum area in the passage (e.g. for turbines throat circle diameter o and angle ϕ in fig. 4a). This defines in turn the suction-surface blade control point P_{sm} and blade angle β_{sm}. The corresponding input values are arbitrary blade point P_{pm} and blade angle β_{pm} on the pressure side for turbines, compressors and airfoils. One major difference of isolated airfoils from compressor and turbine blades is that, on the suction side, P_{sm} and β_{sm} are inputs unrelated to area passage. Other key inputs for isolated airfoils are the LE and TE circle radii (or ellipses, or other

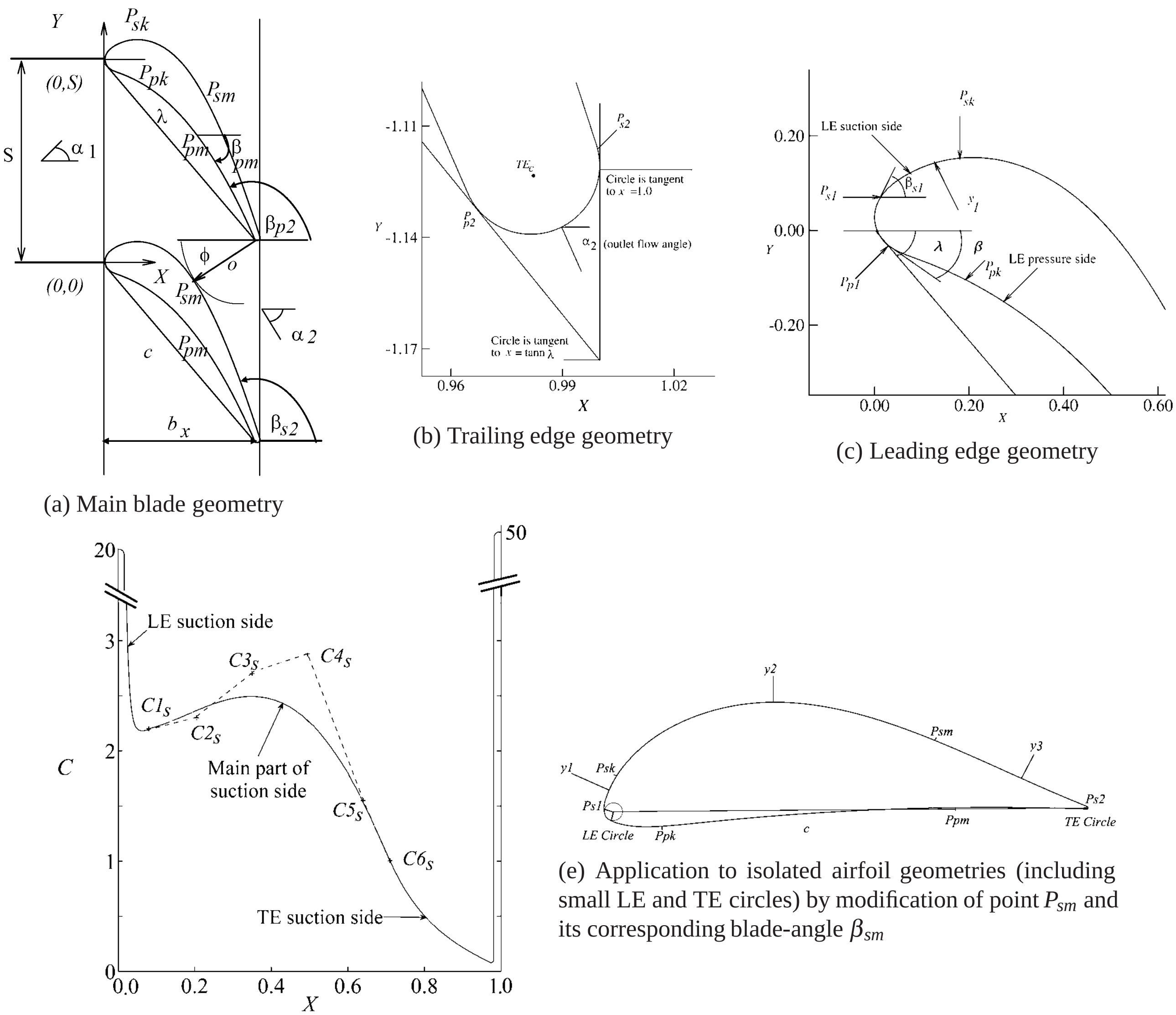

(a) Main blade geometry

(b) Trailing edge geometry

(c) Leading edge geometry

(d) 2D prescribed curvature distribution from leading edge (LE) to trailing edge (TE)

(e) Application to isolated airfoil geometries (including small LE and TE circles) by modification of point P_{sm} and its corresponding blade-angle β_{sm}

FIGURE 4. 2D blade and airfoil geometry definition (adapted from [30, 32])

analytic shapes), and the inlet and outlet flow angles α_1 and α_2. The airfoil-design method presented in this paper illustrates the use of LE and TE circles. These are the hardest shapes to join to the airfoil surfaces as there is a transition from the constant curvature of the circle region to the locally varying curvature of the remaining airfoil surface. Therefore the method presents the most difficult case of joining the LE and TE edge shapes to the rest of the airfoil surface; and all other shapes will be an easier variation of the methodology presented.

The trailing edge radius locates the trailing edge circle (figs. 4b and 4g). The suction and pressure surfaces "detach" from the trailing edge circle at points P_{s2} and P_{p2} specified by input parameters β_{s2} and β_{p2} respectively (local airfoil-surface angles, determined by the "wedge" airfoil angle of the trailing edge, and related to the outlet flow angle α_{ot}). The trailing edge region (line segment $y3$) from P_{s2} to P_{sm} on the suction surface is specified by an analytic polynomial $y = f(x)$ of the form:

$$y3 = f(x) = c_0 + c_1 x + c_2 x^2 + c_3 x^3 + \\ + c_4 k_1[x - x(P_{s2})] + c_5 k_2[x - x(P_{s2})]) \quad (3)$$

where k_1 and k_2 are exponential functions resulting in terms of increasing importance as we approach point P_{s2}, and of negligible importance away from P_{s2}. For example $c_4\, exp\{\Omega[x-x(P_{s2})]\}$, where Ω is a large positive number and $[x-x(P_{s2})]$ is negative, is the simplest form; but many other more complex variations of exponential functions, such as $c_4\, exp\{\Omega\, x^4\, [x-x(P_{s2})]\}$ (increasing the order of the polynomial expressions near points such as P_{s2}) work well. Thus equation 3 is a cubic equation near point P_{sm}; and the basic cubic equation has exponential modifications as it approaches the TE circle at point P_{s2}. The six coefficients c_0 to c_5 are evaluated from the conditions of point, first, second and third derivative continuity (four conditions) of the airfoil surface line at P_{s2}; and prescribing the point and slope of the airfoil surface at P_{sm} (two additional conditions). This approach enables slope of curvature continuity in the vicinity of the trailing edge circle (though the changes in curvature in this vicinity are usually large).

The design of line segment $y2$ between points P_{sm} and P_{sk} is accomplished by "mapping" the curvature distribution for the shape of the blade surface in that region from the $\mathbf{C}$ vs. X plane to the Y vs. X plane using 4-point to 6-point Bezier splines in curvature (fig. 4d). For illustration purposes fig. 4d shows a 6-point Bezier spline, though in principle any n-point Bezier spline can be used, and usually 4 Bezier control points are sufficient. The curvature segment corresponding from P_{s2} to P_{sm} is evaluated from analytic polynomial $y1$ (using eqn. 3) and plotted on the $\mathbf{C}$ vs. X plane starting from the TE at $X = 1.0$ and ending in point $C6s$ in fig. 4d. The slope of the curvature $\mathbf{C}_s(x)$ at point $C6_s$ (corresponding to blade point P_{sm}) is computed from eqn. 3 and becomes an input to further calculations. On the curvature of the suction surface we specify points $C1_s$, to $C5_s$. Point $C1_s$ is specified at an x location corresponding to P_{sk}. Since the slope of the Bezier curve is tangent to the line of knots at its ends, the tangency condition at point $C6_s$ ensures slope-of-curvature continuity from $C1_s$ to $C6_s$ (from P_{sk} to P_{s2}).

Using central differences equation 1 is written for curvature at airfoil point i as a function of (x,y) coordinates of points $i-1, 1$ and $i+1$ [30]. Given (x_{i-1}, y_{i-1}), (x_i, y_i), x_{i+1} and $\mathbf{C}_i$ we can compute y_{i+1} starting from blade points P_{sm} and progressing explicitly point by point towards the leading edge to points P_{sk}. The Bezier spline is iteratively manipulated until the slope and the y location of the airfoil surface at points P_{sk}, and the shape of the curvature distribution, are acceptable.

For consistency among blade designs the points are always specified equidistant from P_{sk} to P_{sm}. Usually points are derived every 0.25% of X at specific locations (e.g. at $X = 0.5100$, next point at $X = 0.5125$, etc.), with additional clustering very near the LE and TE (where the expressions for $y1$ and $y3$ are analytic). More airfoil points may be used for other reasons: numerical machining programs; or depending on the accuracy of the metric terms in the grid generator that will be used for the CFD computations.

In the LE area we implement a hybrid method based on modifications of the earlier methods [28, 30, 32]. First we introduce the leading edge shape, such as a circle or ellipse (fig. 4c). The suction and pressure blade surfaces "detach" from the leading edge circle at points P_{s1} and P_{p1} specified by input parameters β_{s1} and β_{p1} respectively (local blade-surface angles, determining the "wedge" blade angle at the LE). Then a parabolic construction line is defined, and a thickness distribution is added perpendicularly to the construction line (as in [28, 30]). The construction line starts from a key geometric point such as the origin, the leading edge of the blade or the center of the leading edge circle. The thickness distribution is added about this parabolic construction line in a manner that the thickness distribution (and therefore also the blade surface) have continuous point, first, second and third derivative (continuous y, y', y'', y''' and therefore continuous $\mathbf{C}'$) at point P_{s1} where it joins the leading edge shape (circle) and the main part of the blade (point P_{sk} and C_{1s} in figs. 4)c and 4)d. This is analogous to the circle-joining work of [32] with exponentials in the polynomials, and the above trailing-edge region subsection on joining the trailing edge circle to the trailing edge segment of the blade.

The suction-side construction line can be (for instance) of the form:

$$y(x) = Ax^2 + Bx + C \tag{4}$$

and the thickness distribution y_t added perpendicularly to the construction line (in order to subsequently arrive at the coordinates of the leading edge segment $y1$) is of the form

$$\begin{aligned} y_t = \quad & c_0 + c_1 x + c_2 x^2 + c_3 x^3 + \\ & + c_4 k_{11}\,(x - x(P_{s1})) + c_5 k_{12}\,(x - x(P_{sk})) + \\ & + c_6 k_{13}\,(x - x(P_{s1})) + c_7 k_{14}\,(x - x(P_{sk})) \end{aligned} \tag{5}$$

where functions k_{11}, k_{12}, k_{13} and k_{14} are exponential polynomials which acquire increasing importance as we approach points P_{s1} and P_{sk} on the blade surface, so that eq. 5 is a cubic polynomial away from these two end points. The eight parameters of the thickness function c_0 to c_7 are derived from the conditions to match: y, y', y'' and y''' (and thus $\mathbf{C}'$) at point P_{s1}; and at point P_{sk} respectively.

The procedure is similar for the pressure side of the airfoil. This approach ensures continuity of curvature and slope of curvature everywhere on the airfoil surface: from the TE circle; to the main part of the airfoil surface; through the leading-edge thickness distribution; and into the LE circle. The streamwise surface curvature distribution (fig. 4d) is iteratively manipulated to optimize the aerodynamic performance of 2D sections, while keeping control of the airfoil geometry via the direct design method. The designer shapes the surface curvature, and with it the location of maximum loading, forwards or backwards, on the airfoil surface, as described in [31]. After the first iteration (first geometric design and analysis) the user examines the resulting airfoil loading distribution (e.g. C_p) along X, and decides where to increase and decrease local curvature (and local loading). After the second iteration the user gains an appreciation of (or keeps record of) the magnitude of the required changes in curvature to cause the desired changes in C_p distribution along X; or the surface-curvature changes required to improve other design criteria. The procedure is repeated until a desirable airfoil geometry and aerodynamic performance are obtained. The early analysis iterations can start with fast computation methods, such as panel methods; later proceed with more detailed methods, such as Reynolds-averaged Navier-Stokes (RANS) calculations; and even later may also proceed with large-eddy simulations or direct numerical simulations. The above optimization procedure (especially with the relatively-fast panel methods and RANS computations) can be automated with used-defined optimization functions, and simple or complex, visual or codified multi-objective heuristic or evolutionary-algorithm optimization methods in order to optimize various aspects of airfoil geometry or performance, e.g. [47, 48].

The method is easily extended for 3D design of compressor and turbine blade rows as described in [32], by specifying the variation of key 2D blade-design parameters along the blade height in a smooth manner. This is accomplished using the values of each 2D parameter, (for instance 2D parameter $C3_s$, one of the 2D parameters used to specify the suction-surface curvature $\mathbf{C}_s$), at three key 2D sections (hub, mean and tip). We then specify a smooth variation of the same parameter along the blade height with a Bezier curve along the blade height that passes through the value of the 2D parameter at the hub, mean and tip. We then manipulate these Bezier curves of the 2D parameters along the blade height until the 3D geometry exhibits the desired 3D aerodynamic performance. The 3D CIRCLE method is illustrated in previous publications with examples for 3D stacking of gas turbine blades [32], it allows for significant and smoothly-changing variation of airfoil thickness along the blade height, and in principle it can also be used for wind turbines. The resultant smoothly but significantly varying 2D sections can be stacked along the blade center of gravity (for gas turbine and compressor rotor blade rows, for instance). There are additional structural and aerodynamic complexities in stacking 2D airfoil sections for wind turbines. Examples of using the CIRCLE method in 3D wind turbine designs will be presented in future publications.

THE EPPLER AND A2 AIRFOILS

Fig. 5 and Table 1 compare the geometry and design-point ($i_{crd} = +4^\circ$) aerodynamic performance of the original Eppler 387 and of two successfully redesigned airfoils, A1 and A2. Fig. 5a shows a comparison of the three airfoil shapes. A1 and A2 have small TE circles while Eppler has a pointed trailing edge. All three airfoils have the same LE radius, but A1 has a lower LE wedge angle than Eppler, and A2 has a higher LE wedge angle than Eppler (also indicated by the surface curvatures near the LE of the three airfoils in fig. 5b). The curvature distribution of the Eppler airfoil has small "kinks" near the LE at $X \approx 0.01$, and a change in the slope of curvature on the suction surface at $X \approx 0.6$ (fig. 5b). These curvature discontinuities have been removed in the redesigned A1 and A2 airfoils. A1 and A2 have similar performance, but A2 has slightly better computed performance than A1.

Fig. 5c shows the C_p distribution of the Eppler and A2 airfoils. The solid line is the RANS computation of the original airfoil shape, which agrees very well with the experimental data; and the dashed line is the viscous computation of the redesigned A2 airfoil. The $Rey = 10^5$; turbulence intensity is 0.5%; and i_{crd} =+4°. Further experimental details can be found in [49]. The computations used GAMBIT and FLUENT. 2D structured C (for pointed TE Eppler) and O (for circular TE A1 and A2) meshes, with 50 points perpendicular to the airfoil surface (25 to 30 of the 50 points are in the boundary layer thickness), and with 500 to 600 points along the airfoil surface have been used in the computations. These structured grids have clustering around the LE region (the O grid has clustering in the TE region as well), and $y+ \leq 1.2$. The structured grids are surrounded by an unstructured Pave C mesh extending 12 chords upstream and 20 chords downstream of the airfoil, with a total number of about 350,000 grid points. The RANS computations have used the 4-equation $k-\omega$ SST-transition model.

The computed results (fig. 5c) indicate that the removal of the kink in curvature near the LE (near $X = 0.01$) has smoothed the C_p distribution near the LE of airfoils A1 and A2 (magnified region in the C_p distribution). The circle points are the experimental data on the original airfoil (from [49]); the solid line is the RANS computation on the original airfoil shape; and the dashed line is the RANS computation on the redesigned A2 airfoil. The curvature kink in that region of the Eppler airfoil results in a local acceleration-deceleration region of disturbed flow on the suction side of the airfoil (fig. 5d). Unlike the results on the removal of the LE separation bubble of the HD gas-turbine

TABLE 1. Comparison of computed aerodynamic parameters of the Eppler 387 and A2 airfoils with experimental data for the Eppler 387 airfoil

Airfoil	C_L	C_D	C_L/C_D
Eppler (experiment)	0.7778	0.0230	33.82
Eppler (RANS)	0.8007	0.0207	38.68
A1 (RANS)	0.7591	0.0181	41.94
A2 (RANS)	0.7276	0.0172	42.30

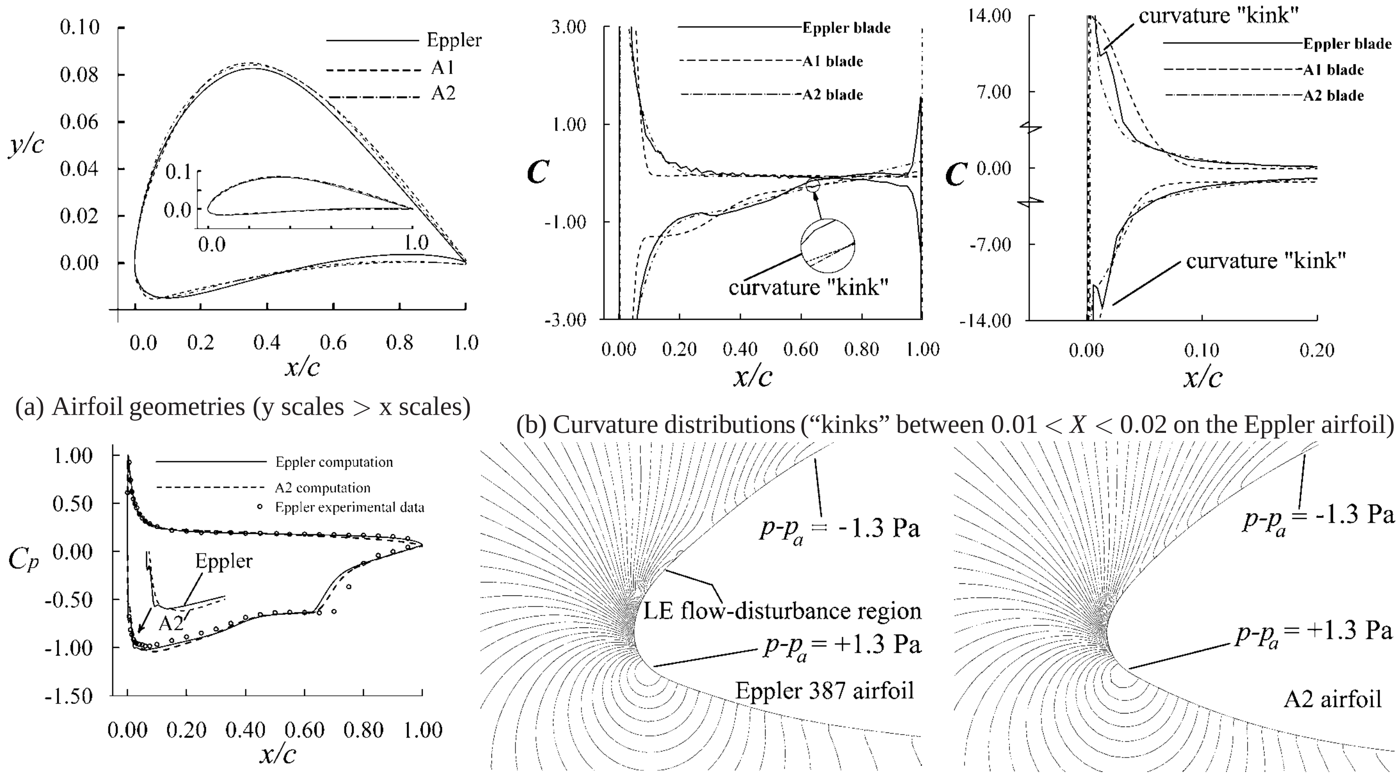

(a) Airfoil geometries (y scales > x scales)

(b) Curvature distributions ("kinks" between $0.01 < X < 0.02$ on the Eppler airfoil)

(c) C_p distributions

(d) Eppler airfoil: p contours near the LE

(e) A2 airfoil: p contours near the LE

FIGURE 5. Comparison of Eppler 387, A1 and A2 airfoils

blade presented in [45], the computed results indicate this flow disturbance on the LE of the Eppler airfoil is not a separation bubble (at this value of incidence and this *Rey* and incoming turbulence level). In this case the flow disturbance is just a local flow acceleration-deceleration, which nevertheless disturbs the local boundary layer behavior. The removal of the surface curvature kink in that region results in smooth accelerating flow in the same region of the A2 airfoil (figs. 5c, 5e). Use of the CIRCLE method can be used to remove the LE "kink" in curvature, and thus eliminate the sharp acceleration-deceleration flow regions in the LE of airfoils, replacing this with a smooth and continuously accelerating flow. This is illustrated for a mid-range incidence for the Eppler 387 and A2 airfoils in fig. 5c, and in [45] for the HD and B3 blades (the latter at design and off-design incidences). This is related to the double-stall phenomenon in airfoils for incidences near maximum lift, and airfoil redesign to reduce this effect, as in [23]. Double stall may be attributed to laminar separation bubbles near the LE at these high incidences undergoing cycles of bursting and re-establishment, resulting in two significantly different levels in airfoil lift at identical inflow conditions [21, 22]. The LE disturbances may not cause laminar separation bubbles in higher *Rey* airfoils of current wind turbines, but removal of the curvature kink at the LE facilitates smoother boundary layer development over the LE region.

The RANS computations (fig. 5c) indicate that, when the Eppler 387, A1 and A2 airfoils operate at $Rey = 10^5$, the boundary layer remains laminar until about $X \approx 0.6$. After that the momentum of the boundary layer near the surface is insufficient to carry the flow, and there is a laminar separation bubble in that region. The RANS computations indicate that the flow re-attaches turbulent further downstream. However, the laminar separation in that region of the airfoils is a characteristic of the Reynolds number of the flow and the diffusion required by the airfoils (Eppler, A1 and A2). Both airfoils A1 and A2 have removed the small change in the slope of curvature that occurs at $X \approx 0.6$ in the Eppler airfoil (fig.5b); but the smooth curvatures of A1 and A2 cannot change the nature of the flow, and cannot prevent the laminar separation in that region. Nevertheless, the computations indicate that smoothing of the curvature from the LE region and throughout the airfoil surface has a beneficial effect on performance. At $i_{crd} = 4°$ the computations indicate that the reattachment point of the Eppler airfoil is at $X = 0.677$; of A1 is at $X = 0.680$; of A2 is at $X = 0.682$. The corresponding airfoil wakes are progressively thinner, reflected in a drop in computed C_D from 0.0207 to 0.0172, and a corresponding rise of C_L/C_D from 38.68 to 42.30 (Table 1).

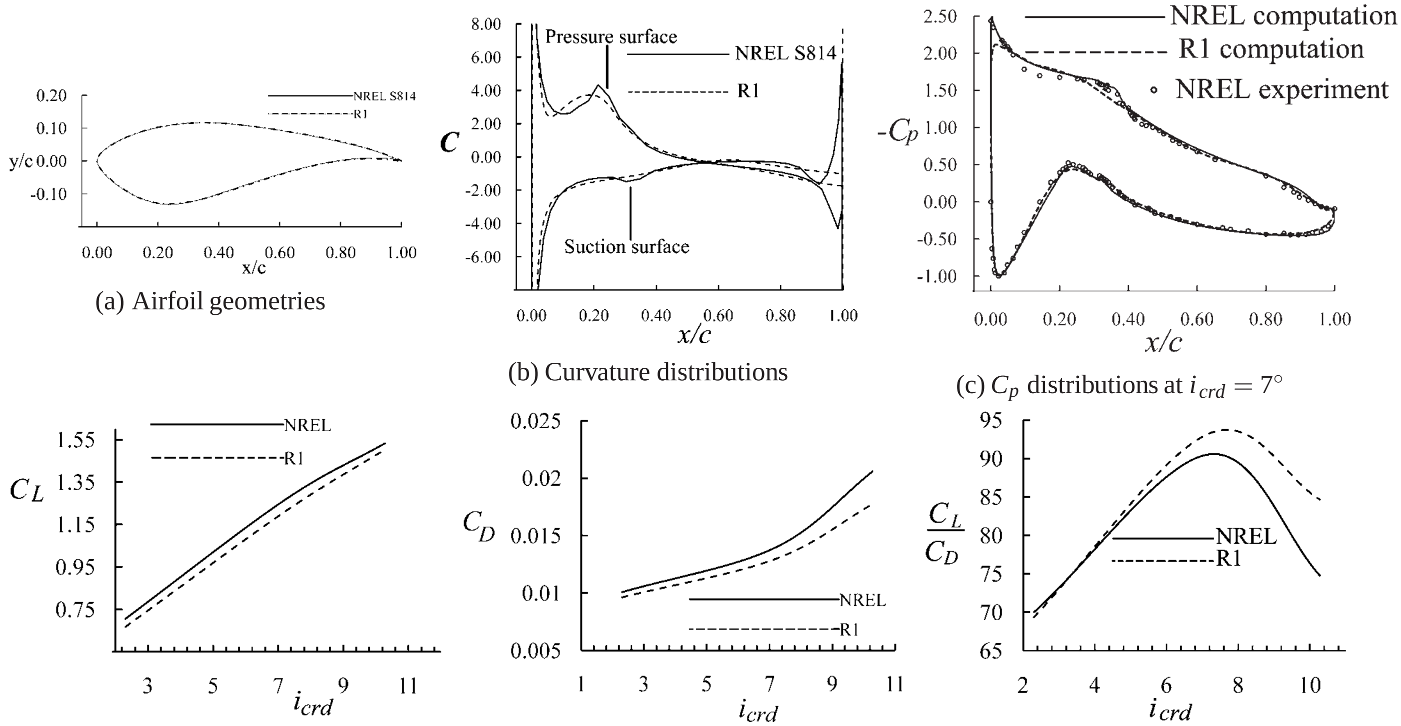

(a) Airfoil geometries (b) Curvature distributions (c) C_p distributions at $i_{crd} = 7°$

(d) C_L distributions (e) C_D distributions (f) C_L/C_D distributions

FIGURE 6. Comparison of NREL S814 and R1 airfoils

THE NREL S814 AND R1 AIRFOILS

Fig. 6 shows a comparison of the geometry, design-point ($i_{crd} = +7.19°$), and off-design incidence aerodynamic performance of the original NREL S814 airfoil (designed for wind-turbine near-hub sections) and of redesigned airfoil R1. R1 has a small TE circle while S814 has a pointed trailing edge. Both airfoils have the same LE radius. The curvature distribution of the NREL S814 airfoil has small "kinks" near $X \approx 0.2$ on the pressure surface and near $X \approx 0.3$ on the suction surface. (fig. 6b). These curvature discontinuities, as well as a LE spike, have been removed in the redesigned R1 airfoil.

Fig. 6c shows the C_p distribution of the S814 and R2 airfoils at design incidence. The solid line is the RANS computation of the original airfoil shape, which agrees very well with the experimental data, and the dashed line is the viscous computation of the redesigned R1 airfoil. The Rey=1.5×10^6; and turbulence intensity is 2.5%, so that the flow over the airfoil is turbulent. Further experimental details can be found in [50]. The RANS computations were performed with FLUENT. 2D structured C (for pointed TE S814) and O (for circular TE R1) meshes, with 50 points perpendicular to the airfoil surface (25 to 30 of the 50 points are in the boundary layer thickness), and with 500 to 600 points along the airfoil surface have been used in the computations. These structured grids have clustering around the LE region (the O grid has clustering in the TE region as well), and $y+ \leq 1.2$. The structured grids are surrounded by an unstructured Pave C mesh extending 12 chords upstream and 20 chords downstream of the airfoil, with a total number of about 380,000 grid points. The 4-equation $k-\omega$ SST-transition model was used in the RANS computations.

The results (fig. 6c) indicate the removal of the small "bumps" in curvature near $X \approx 0.2$ on the pressure surface, and near $X \approx 0.3$ on the suction surface, has resulted in removal of the small corresponding "bump" regions in the C_p distributions in those locations. These effects are always more visible on the suction surfaces where the flow velocities are higher. Furthermore, the smoothing of the curvature near the LE of the R1 airfoil has resulted in replacement of the C_p spike in that location with a smooth C_p distribution.

The differences in surface curvature distributions of comparable airfoils along their chord (e.g. such as NREL S814 and R1) dictate the differences in airfoil geometry, as well as the differences in local loading (C_p) distributions along their chord. The correlation between surface curvature, airfoil geometry, and C_p or pressure distribution along X is more visible in the examples of gas turbine blades included in [31], because the surface curvatures in gas turbine blades are higher than those in most isolated airfoils. The relative effects of surface-curvature differences are smaller, but follow the same patterns in airfoils.

For example, the curvature of the NREL S814 airfoil is lower than the curvature of airfoil R1 on the suction surface between $0.28 < X < 0.4$, and higher between $0.10 < X < 0.28$ on the same surface (fig. 6b; the curvature values are negative). This means the surface of NREL S814 is more rounded than the surface of R1 between $0.28 < X < 0.4$. This results in the C_p distribution of NREL S814 to be higher than the C_p distribution of R1 in the same vicinity $0.28 < X < 0.4$. (We used this shape of curvature on airfoil R1 in the vicinity of $0.28 < X < 0.4$ in order to remove the "bump" in the C_p distribution of NREL S814, fig. 6c). The situation is reversed between $0.10 < X < 0.28$, where the surface curvature of R1 is slightly lower than NREL S814, and the C_p of R1 is slightly higher than that of NREL S814.

Figs. 6d to 6f show comparisons of C_L, C_D and C_L/C_D versus i_{crd} from the RANS computations on the original S814 and redesigned R1 airfoils. These computed results indicate that, at design and off-design incidence, although there is a small reduction in C_L, C_D is reduced correspondingly more, because of reduction of friction losses on the airfoil surfaces, resulting from the removal of the surface curvature "kinks". This reduction in C_D results in improvement of C_L/C_D practically throughout the range of incidence in fig 6f.

CONCLUSIONS

The CIRCLE method was originally developed for the design of 2D and 3D subsonic, transonic or supersonic blades for axial compressors and turbines. Starting from flow specifications, it has been used for the design of about 30 2D compressor and turbine blades, and 3 3D compressor and turbine blade rows in previous work, as well as for the redesign modification of various existing blade geometries. This paper illustrates the extension of the original method to the redesign of two 2D airfoils used in wind turbines, and describes the use of the method for 2D and 3D original airfoil and blade designs for wind turbines.

The CIRCLE method, which can be easily coupled to multi-objective heuristic or evolutionary-algorithm optimization methods, is based on prescribing the smooth and continuous streamwise 2D suction- and pressure-surface curvatures from leading to trailing edge of the blades or airfoils. This curvature and slope of curvature continuity includes the locations where the suction and pressure surfaces join the leading and trailing edge circles, ellipses, or other shapes, so that curvature and slope of curvature are smooth and continuous everywhere along the airfoil surfaces from nominal LE point to nominal TE point, as well as everywhere around the airfoil surface (throughout 360°). In the 3D method the 2D sections of the hub, mean and tip (or near hub and tip) are designed first. Then the 2D airfoil-design parameters are smoothly varied from hub to tip with Bezier curves in the radial direction, providing a smooth variation of 2D sections from hub to tip, and allowing significant changes in 2D thickness along the blade height. The method can be further enhanced using the results of 2D or 3D flow computations coupled to optimization methods to direct the variation of the airfoil- or blade-design parameters. The 3D CIRCLE method in principle can be used for the design of 3D wind turbine blades (though this aspect is not addressed in this paper).

This is a new design environment decoupling the traditional maximum thickness and maximum camber discussions (used in early airfoil designs) from airfoil-section design, and it attaches greater significance to the curvature distribution rather than the exact location of (x, y) points on the airfoil, even though the designer has direct control of the airfoil surface as in direct methods. Similarly to inverse design methods, the CIRCLE method is guided by the surface pressure distributions with their relation to surface-curvature distributions, and the output is the airfoil shape. The design sequence shapes the surface curvature and with it the location of maximum loading, forwards or backwards, on the airfoil surface. Therefore this method combines the best advantages of direct and inverse airfoil design methods.

The aerodynamic advantages of the CIRCLE airfoil design method in designing improved wind turbine airfoils (of lower losses and higher lift-to-drag ratios) are illustrated with two examples of 2D airfoils of known tested experimental performance: the Eppler 387; and the NREL S814. The modified airfoils are practically identical in section geometry to the original ones. The surface curvature distributions and C_p distributions of the modified airfoils are smoother than those of the original ones. The flow performance of the original and modified airfoils are analyzed with CFD, and the computed performance advantages of the redesigned 2D airfoils are discussed.

The redesigned airfoils have removed leading-edge flow-disturbance regions from both original airfoils, a mid-chord suction-surface flow-disturbance region from the Eppler 387 airfoil, and mid-chord pressure- and suction-surface flow-disturbance regions from the NREL S814 airfoil. The modified airfoils have lower computed drag coefficients, and higher lift-to-drag coefficients than the original ones. It is concluded that the method is a new and efficient design tool in the arsenal for the tailoring of existing airfoils to increase efficiency for wind-turbine airfoils. Design of new airfoils is also possible, but is not shown in this paper.

Fig. 5a indicates that the differences in airfoil surface geometries are of a magnitude that is measurable in the chord sizes of modern large wind turbines. However, more importantly, figs. 5b, 5c, 6b and 6c indicate that, in addition to the usual surface-geometry point-by-point measurement of manufacturing tolerances, we need to introduce additional measurements of acceptable tolerances in airfoil-surface curvature distribution.

ACKNOWLEDGMENT

The authors acknowledge the contributions of MSc and PhD students, and postdocs, who over two decades have contributed to coding various aspects of the CIRCLE blade design method in FORTRAN, C++ and MATLAB, and on various platforms and operating systems: George Pantazopoulos; Nick Vlachopoulos; Paschalis Papagiannidis; Dequan Zou; Richard Binzley; Sean Spicer; Brandon Wegge; Yan Tan; Mingyu Shi; and Akbar Rahideh. The PhD research of Idres Hamakhan was sponsored by the Ministry of Education of Kurdistan; and the PhD research of M. Amin Rezaienia is currently sponsored by Queen Mary, University of London.

REFERENCES

[1] Devinant, P., Laverne, T., and Hureau, J., 2002. "Experimental study of wind-turbine airfoil aerodynamics in high turbulence". *Journal of Wind Engineering and Industrial Aerodynamics,* ***90***(6), Jun, pp. 689–707.

[2] Lissaman, P. B. S., 1983. "Low-Reynolds-number airfoils". *Annual Review of Fluid Mechanics,* ***15***, pp. 223–239.

[3] Hansen, A. C., and Butterfield, C. P., 1993. "Aerodynamics of horizontal axis wind turbines". *Annual Review of Fluid Mechanics,* ***25***, pp. 115–149.

[4] Bertagnolio, F., Sorensen, N., Johansen, J., and Fuglsang, P., 2001. Wind turbine airfoil catalogue. Risø National Laboratory Report Risø-R-1280(EN).

[5] Fuglsang, P., Bak, C., Gaunaa, M., and Antoniou, I., 2003. Wind tunnel tests of Risø-B1-18 and Risø-B1-24. Risø National Laboratory Report Risø-R-1375(EN).

[6] Ameku, K., Nagai, B. M., and Roy, J. N., 2008. "Design of a 3 kW wind turbine generator with thin airfoil blades". *Experimental and Thermal and Fluid Science,* ***32***(8), Sep, pp. 1723–1730.

[7] Habali, S. M., and Saleh, I. A., 1995. "Design and testing of small mixed airfoil wind turbine blades". *Renewable Energy,* ***6***(2), pp. 161–169.

[8] Selig, M. S., and Maughamer, M. D., 1992. "Multipoint inverse airfoil design method based on conformal mapping". *AIAA Journal,* ***30***(5), May, pp. 1162–1170.

[9] Selig, M. S., and Mughamer, M. D., 1992. "Generalized multipoint inverse airfoil design". *AIAA Journal,* ***30***(11), Nov, pp. 2618–2625.

[10] Dahl, K. S., and Fuglsang, P., 1998. Design of the wind turbine airfoil family Risø-A-xx. Risø National Laboratory Report Risø-R-1024(EN).

[11] Li, J. Y., Li, R., Gao, Y., and Huang, J., 2010. "Aerodynamic optimization of wind turbine airfoils using response surface techniques". *Proceedings of the Institution of Mechanical Engineers - Part A-Journal Of Power and Energy,* ***224***(A6), pp. 827–838.

[12] Selig, M. S., 1994. "Multipoint inverse design of an infinite cascade of airfoils". *AIAA Journal,* ***32***(4), Apr, pp. 774–782.

[13] Dang, T., Damle, S., and Qiu, X., 2000. "Euler-based inverse method for turbomachine blades, Part 2: Three-dimensional flows". *AIAA Journal,* ***38***(11), Nov, pp. 2007–2013.

[14] Liu, G.-L., 2000. "A new generation of inverse shape design problem in aerodynamics and aero-thermoelasticity: concepts, theory and methods". *An International Journal of Aircraft Engineering and Aerospace Technology,* ***72***(4), April, pp. 334–344.

[15] Phillipsen, B., 2005. A simple inverse cascade design method. ASME paper 2005-GT-68575.

[16] Brear, M. J., and Hodson, H. P., 2003. "The response of a laminar separation bubble to 'aircraft engine representative' freestream disturbances". *Experiments in Fluids,* ***35***(6), Dec, pp. 610–617.

[17] Geissler, W., and Haselmeyer, H., 2006. "Investigation of dynamic stall onset". *Aerospace Science and Technology,* ***10***(7), Oct, pp. 590–600.

[18] Traub, L. W., and Cooper, E., 2008. "Experimental investigation of pressure measurement and airfoil characteristics at low Reynolds numbers". *Journal of Aircraft,* ***45***(4), Jul-Aug, pp. 1322–1333.

[19] Savaliya, S. B., Kumar, S. P., and Mittal, S., 2010. "Laminar separation bubble on an Eppler 61 airfoil". *International Journal for Numerical Methods in Fluids,* ***64***(6), Oct, pp. 627–652.

[20] Henderson, A. D., and Walker, G. J., 2010. "Observations of Transition Phenomena on a Controlled Diffusion Compressor Stator With a Circular Arc Leading Edge". *Transactions of the ASME, Journal of Turbomachinery,* ***132***(3), Jul, pp. 031002–1 to –9.

[21] Bak, C., Madsen, H. A., Fuglsang, P., and Rasmussen, F., 1998. Double stall. Risø National Laboratory Report Risø-R-1043(EN).

[22] Bak, C., Madsen, H. A., Fuglsang, P., and Rasmussen, F., 1999. "Observations and hypothesis of double stall". *Wind Energy,* ***2***(4), Oct/Dec, pp. 195–210.

[23] Bak, C., and Fuglsang, P., 2002. "Modification of the NACA 63(2)-415 leading edge for better aerodynamic performance". *ASME Journal of Solar Energy Engineering,* ***124***(4), Nov, pp. 327–334.

[24] McMasters, J. H., and Henderson, M. L., 1980. "Low speed single element airfoil synthesis". *Tech. Soaring,* ***6***(2), pp. 1–21.

[25] Leipold, R., Boese, M., and Fottner, L., 2000. "The influence of technical surface roughness caused by precision forging on the flow around a highly loaded compressor cascade". *Transactions of the ASME, Journal of Turbomachinery,* ***122***(3), Jul, pp. 416–424.

[26] Montomoli, F., Hodson, H., and Haselbach, F., 2010. "Effect of Roughness and Unsteadiness on the Performance of a New Low Pressure Turbine Blade at Low Reynolds Numbers". *Transactions of the ASME, Journal of Turbomachinery,* ***132***(3), Jul, pp. 031018–1 to –9.

[27] Korakianitis, T., 1987. “A design method for the prediction of unsteady forces on subsonic, axial gas-turbine blades”. Doctoral dissertation (Sc.D., MIT Ph.D.) in Mechanical Engineering, Massachusetts Institute of Technology, Cambridge, MA, USA, September.

[28] Korakianitis, T., 1989. “Design of airfoils and cascades of airfoils”. *AIAA Journal*, ***Vol.27***(4), April, pp. 455–461.

[29] Korakianitis, T., 1993. “Hierarchical development of three direct-design methods for two-dimensional axial-turbomachinery cascades”. *Journal of Turbomachinery, Transactions of the ASME*, ***115***(2), April, pp. 314–324.

[30] Korakianitis, T., 1993. “Prescribed-curvature distribution airfoils for the preliminary geometric design of axial turbomachinery cascades”. *Journal of Turbomachinery, Transactions of the ASME*, ***115***(2), April, pp. 325–333.

[31] Korakianitis, T., and Papagiannidis, P., 1993. “Surface-curvature-distribution effects on turbine-cascade performance”. *Journal of Turbomachinery, Transactions of the ASME*, ***115***(2), April, pp. 334–341.

[32] Korakianitis, T., and Wegge, B. H., 2002. Three dimensional direct turbine blade design method. AIAA paper 2002-3347. AIAA 32nd fluid dynamics conference and exhibit, St. Louis, Missouri, June.

[33] Okapuu, U., 1974. Some results from tests on a high work axial gas generator turbine. ASME paper 74-GT-81, March.

[34] Gostelow, J. P., 1976. A new approach to the experimental study of turbomachinery flow phenomena. ASME paper 76-GT-47.

[35] Wagner, J. H., Dring, R. P., and Joslyn, H. D., 1984. Inlet boundary layer effects in an axial compressor rotor: part 1 - blade-to-blade effects. ASME paper 84-GT-84.

[36] Sharma, O. P., Pickett, G. F., and Ni, R. H., 1990. Assessment of unsteady flows in turbines. ASME paper 90-GT-150.

[37] Hourmouziadis, J., Buckl, F., and Bergmann, P., 1987. The development of the profile boundary layer in a turbine environment. Transactions of the ASME, Journal of Turbomachinery, Volume 109, No. 2, pp. 286-295, April. ASME paper 86-GT-244, 1986.

[38] Hodson, H. P., and Dominy, R. G., 1987. “Three-dimensional flow in a low pressure turbine cascade at its design condition”. *Transactions of the ASME, Journal of Turbomachinery*, ***109***(2), Apr, pp. 177–185. ASME paper 86-GT-106.

[39] Hodson, H. P., and Dominy, R. G., 1987. “The off-design performance of a low-pressure turbine cascade”. *Transactions of the ASME, Journal of Turbomachinery*, ***109***(2), Apr, pp. 201–209. ASME paper 86-GT-188.

[40] Hodson, H. P., 1985. “Boundary-layer transition and separation near the leading edge of a high-speed turbine blade”. *Transactions of the ASME, Journal of Engineering for Gas Turbines and Power*, ***107***, pp. 127–134. ASME paper 84-GT-179.

[41] Goodhand, M. N., and Miller, R. J., 2011. “Compressor leading edge spikes: a new performance criterion”. *Transactions of the ASME, Journal of Turbomachinery*, ***133***(2), April, pp. 021006–1 021006–8.

[42] Wheeler, A. P. S., Sofia, A., and Miller, R. J., 2009. “The effect of leading-edge geometry on wake interactions in compressors”. *Transaction of the ASME, Journal of Turbomachinery*, ***131***(4), pp. 041013–1 – 041013–8.

[43] Stow, P., 1989. “Blading design for multi-stage hp compressors”. In *Blading design for axial turbomachines, AGARD Lecture Series 167, AGARD-LS-167*. AGARD, May.

[44] Corral, R., and Pastor, G., 2004. “Parametric design of turbomachinery airfoils using highly differentiable splines”. *Journal of Propulsion and Power, Vol. 20, No. 2, pp. 335-343*, March-April.

[45] Hamakhan, I. A., and Korakianitis, T., 2010. “Aerodynamic performance effects of leading edge geometry in gas turbine blades”. *Applied Energy*, ***87***(5), May, pp. 1591–1601.

[46] Korakianitis, T., Hamakhan, I. A., Rezaienia, M. A., and Wheeler, A. P. S., 2011. Two- and three-dimensional prescribed surface curvature distribution blade design (CIRCLE) method for the design of high efficiency turbines, compressors, and isolated airfoils. ASME paper GT2011-46722, ASME Turbo Expo, Vancouver, Canada.

[47] Kim, H., Koc, S., and Nakahashi, K., 2005. “Surface modification method for aerodynamic design optimization”. *AIAA Journal*, ***43***(4), Apr, pp. 727–740.

[48] Samad, A., and Kim, K. Y., 2008. “Shape optimization of an axial compressor blade by multi-objective genetic algorithm”. *Proceedings of the Institution of Mechanical Engineers part A-Journal of Power and Energy*, ***222***(A6), Sep, pp. 599–611.

[49] McGhee, R. J., and Walker, B. S., 1988. Experimental results for the Eppler 387 airfoil at low Renolds numbers in the Langley Low Pressure Turbine Tunnel. NASA-TM-4062.

[50] Somers, D. M., 1997. Design and experimental results for the S814 airfoil. National Renewable Energy Laboratory report NREL/SR-440-6919, Jan.